Lab on a Chip

RSC Publishing

PAPER

View Article Online
View Journal | View Issue

Cite this: *Lab Chip*, 2013, **13**, 2300

A microfluidic impedance flow cytometer for identification of differentiation state of stem cells

Hongjun Song,[a] Yi Wang,*[a] Jenna M. Rosano,[a] Balabhaskar Prabhakarpandian,[a] Charles Garson,[a] Kapil Pant[a] and Eva Lai[bc]

Received 30th November 2012,
Accepted 25th March 2013

DOI: 10.1039/c3lc41321g

www.rsc.org/loc

This paper presents a microfluidic electrical impedance flow cytometer (FC) for identifying the differentiation state of single stem cells. This device is comprised of a novel dual micropore design, which not only enhances the processing throughput, but also allows the associated electrodes to be used as a reference for one another. A signal processing algorithm, based on the support vector machine (SVM) theory, and a data classification method were developed to automate the identification of sample types and cell differentiation state based on measured impedance values. The device itself was fabricated using a combination of standard and soft lithography techniques to generate a PDMS-gold electrode construct. Experimental testing with non-biological particles and mouse embryonic carcinoma cells (P19, undifferentiated and differentiated) was carried out using a range of excitation frequencies. The effects of the frequency and the interrogation parameters on sample identification performance were investigated. It was found that the real and imaginary part of the detected impedance signal were adequate for distinguishing the undifferentiated P19 cells from non-biological polystyrene beads at all tested frequencies. A higher frequency and an opacity index were required to resolve the undifferentiated and differentiated P19 cells by capturing capacitive changes in electrophysiological properties arising from differentiation. The experimental results demonstrated salient accuracy of the device and algorithm, and established its feasibility for non-invasive, label-free identification of the differentiation state of the stem cells.

1 Introduction

Stem cell research is one of the most promising medical treatment strategies to be discovered and utilized in modern medicine. Stem cell therapy has wide ranging applications from treating diseases, such as cancer and diabetes, to cell repair therapies for wound healing following trauma.[1] Recent breakthroughs in stem cell technology have established adult pluripotent stem cells as a promising alternative to embryonic stem cells, thereby side-stepping the ethical issues associated with using human embryonic stem cells.[2] The primary step in using stem cells is to direct the differentiation of the cells to the desired progeny. For example, stem cells can be differentiated under controlled conditions to produce cells of any of the three germ layers – ectoderm, mesoderm or endoderm. At regular time points during the differentiation process, the cell population is monitored for presence of the respective germ layer cells.

Biochemical assays, including reverse transcription-polymerase chain reaction (RT-PCR), quantitative PCR (qPCR) and microarrays, have been developed for monitoring the differentiation state of stem cells.[3] However, most of these assays use dedicated, bulky instruments, and are time-consuming, labor-intensive, and consumable-demanding. In addition, these methods are invasive, *i.e.*, they alter, damage or destroy the cell sample. To mitigate such side effects, non-invasive methods are highly desired for monitoring the stem cell differentiation process. Although microscopic observation is commonly used to non-invasively monitor phenotypic changes typical of differentiated stem cells, this method is time and skilled labor intensive, and lacks the power of quantitative analysis. Fluorescence activated cell sorting (FACS), using fluorescent antibodies at a single cell level, has also been used to characterize stem cell differentiation.[4] However, FACS requires cell surface modification by fluorescent biomarkers or antibodies, which may alter cellular properties. In addition, the instrumentation burden for optical detection is rather expensive and complex.

In contrast, electrical impedance-based cellular analysis is a label-free, non-invasive technology, and has been widely used

[a]*CFD Research Corporation, 215 Wynn Drive, Huntsville, AL, 35805, USA. E-mail: yxw@cfdrc.com; Fax: +1 256-327-0985; Tel: +1 256-327-0678*
[b]*Department of Chemical and Biomolecular Engineering, Johns Hopkins University, 3400 N. Charles Street, Baltimore, MD 21218, USA*
[c]*Telemedicine and Advanced Technology Research Center (TATRC), U.S. Army Medical Research and Materiel Command (USAMRMC), 1054 Patchel Street, Fort Detrick, MD 21702, USA*

to analyze and identify cell characteristics in various applications, such as tissue culture,[5–7] cell viability,[8,9] cell growth,[10] cytotoxicity[11] and, more recently, for neural differentiation.[12] The advent of microfluidic (also termed ''lab-on-a-chip'') technologies enables an elegant way of integrating the analytical processes involved in sample preparation, manipulation, and impedance-based detection onto monolithic chips. Microfluidic technology not only renders the system highly compact, but also minimizes size, weight, and power (SWaP) requirements as well as user intervention, making it a highly autonomous system. Microfluidic impedance detection exploits microfabricated electrodes in microchannels/microchambers to sense minute variations in impedance caused by morphological and electrophysiological changes within the cells. It should be noted that the dielectric properties such as the membrane capacitance and cytoplasmic conductivity are governed by the morphological and electrophysiological changes that accompany cell differentiation. Hence, impedance-based analysis is well-suited for monitoring and characterizing differentiation states of cells.

Impedance-based cellular analysis can be classified into two categories: (1) electrical impedance spectroscopy (EIS) and (2) microfluidic flow cytometry (FC). In an EIS microchip, impedance measurements are acquired at a wide range of frequencies within a static environment (no flow). Single cells or cell aggregates are either trapped in a fixed position or adhered onto the surface of the microchip. Bieberich and Guiseppi-Elie[13] used EIS to non-invasively monitor differentiation of PC12 and embryonic stem cells into neurons by interfacing the cells with an interdigitated microelectrode array. Cho *et al.* developed a chip-based EIS system to detect the effects of herpes simplex viruses on Vero cells,[14] and to monitor toxic effects of pesticides on stem cell differentiation.[15] Hildebrandt *et al.*[14] utilized EIS for non-invasive and time-continuous monitoring of the osteogenic differentiation of human mesenchymal stem cells. Dalmay *et al.*[15] developed an ultra-sensitive biosensor based on EIS at microwave frequency range for biological cell discrimination. The sensor design takes advantage of microwave filter architecture to enhance sensitivity. Bagnaninchi *et al.*[16] presented real time label-free monitoring of adipose-derived stem cells differentiation using an EIS chip with microelectrode array. The results demonstrated that the osteoblast and adipocyte lineages have distinct dielectric properties which can be used to discern stem cell differentiation status. The aforementioned studies using microelectrode array-based EIS are limited to measuring population-based cell impedance, rather than identifying the differentiation state of single cells. Recent studies have attempted to modify EIS for single cell analysis by combining the electrode array with microfluidic cell docking/trapping of single cells. Cho *et al.*[17] were able to successfully distinguish the metastatic status of single head and neck cancer cells by trapping individual cells in a docking structure before measuring the impedance.

In the microfluidic flow cytometry (FC) domain, single cells continuously flow between electrode pairs energized with AC excitation signals at one or multiple frequencies. Since the area enclosed by the electrode pair approaches the diameter of the cells, minute electrophysiological variations at the single cell level can be detected and correlated to the impedance measurements.[18] Gawad *et al.*[19] developed a spectral impedance FC micro-analyzer for individual cell sizing and analysis, with a screening rate over 100 cells s^{-1}. A dielectric model of this system was also developed using 3D finite element method in order to determine the influence of different cell properties, such as size, membrane capacitance and cytoplasm conductivity, on the impedance spectrum.[20] Cheung *et al.* presented a microfluidic impedance-based FC system for rapid dielectric characterization of different cells and particles including polystyrene beads, red blood cells (RBCs), ghosts, and RBCs fixed in glutaraldehyde within a simple microfluidic channel.[21] The impedance was measured for single cells at two simultaneously applied frequencies, and the amplitude, phase, and opacity index were used to distinguish cells. The results show that RBCs and ghosts could be differentiated based on phase, whereas the opacity was a more appropriate parameter for distinguishing RBCs from RBCs fixed in glutaraldehyde. Küttel *et al.*[22] successfully detected *Babesia bovis* infected red blood cells using a microfabricated impedance-based FC system by identifying alterations in impedance attributed to cell death and changes in membrane potential or intracellular free Ca^{2+}. Holmes *et al.*[23] demonstrated a microfluidic impedance-based FC for blood cell differential count. The results show accurate impedance identification of T-lymphocytes, monocytes and neutrophils using dual frequencies, which is confirmed by simultaneous fluorescence measurements. Subsequently, Holmes and Morgan[24] distinguished and quantified a CD4 T-lymphocyte sub-population within human whole blood using a similar approach. Pierzchalski *et al.*[25] used microfluidic impedance FC to characterize eukaryotic cell viability and physiology. Gou *et al.*[26] designed and fabricated a T-shaped microchannel with a pair of gold electrodes located horizontally on each side of the microchannel to successfully identify HL-60 and SMMC-7721 cells, as well as discriminate between normal, apoptotic and necrotic SMMC-7721 cells in flow.

The aforementioned devices all employ electrode pairs in a uniform microchannel with a cross-sectional size comparable to the size of the cells. Typically, a microfluidic (hydrodynamic or electrokinetic) focuser is needed to focus the cells in a single file to reduce data scattering and enhance sensitivity of single cell impedance measurements, especially for small size particles and bacteria. Bernabini *et al.*[27] presented a microfluidic impedance FC, which focuses the sample stream in the middle of the channel using an insulating sheath flow, and detects and differentiates 2 μm beads and *E. coli*. The focused sample stream significantly reduces the sensing area, thereby increasing the sensitivity. Alternatively, a micropore feature with a pore size comparable to the diameter of the cells can be built within a large microchannel to improve the detection sensitivity and reliability (in a spirit similar to a Coulter

counter). The physical insulating structure around a micropore plays an equivalent role as the insulating sheath flow in the hydrodynamic focusing design to reduce the sensing area, and hence, minimizes data scattering. Saleh *et al.*[28] developed a micropore-based high sensitivity counter to detect nanoscale colloids by measuring the resistance change near the micropore. The device was able to detect colloids as small as 87 nm, and distinguish colloids whose diameters differ by less than 10%. Satake *et al.*[29] developed a micropore-based sensor to count blood cells and successfully distinguish between RBCs and white blood cells (WBCs). Zheng *et al.*[30] reported a microfluidic impedance FC using a constriction channel that is marginally smaller than the diameter of the cells to characterize RBCs. The system demonstrated a higher throughput and signal to noise (S/N) ratio than the previous devices for single RBC biophysical measurements. Zheng *et al.*[31] also used a similar device to determine the specific membrane capacitance and cytoplasm conductivity of single cells. Differences in membrane capacitance and cytoplasm conductivity between AML-2 cells and HL-60 cells were clearly observed, enabling additional information for enhanced cell discrimination.

For accurate data analysis and cell discrimination/classification, van Berkel *et al.*[32] introduced a 2D Gaussian distribution function to automated fitting of the impedance data for different cells. This approach provided classification boundaries, which mark the positions of equal probability deviation to obtain an accurate count of different cells (*e.g.*, lymphocytes, granulocytes and monocytes in their study). Recently machine learning methods have also been used to enhance data analysis in biological and chemical applications, including several efforts in microfluidic impedance measurements. A two-layer back propagation artificial neural network (ANN) has been reported to quantitatively distinguish between the EMT6 and the EMT6/AR1.0 cells,[33] as well as between fetal/neonatal and adult RBCs.[30]

In this paper, we present a novel methodology that combines a micropore design and electrical impedance based flow cytometer for identifying and characterizing the differentiation state of stem cells. Our microfluidic device utilizes an innovative, dual micropore configuration that not only enhances the processing throughput, but also allows each individual pore and corresponding electrode pair to be used as the reference for the other. Additionally, the design mitigates the reliance on an additional focusing step to minimize data scattering. A signal processing algorithm based on support vector machine (SVM) classification was developed to enable the identification of cell types and differentiation state based on their measured impedance values. The performance of the microfluidic impedance FC device and associated signal processing algorithm was demonstrated by characterizing the differentiation state of a mouse embryonic carcinoma cell line, P19. The cells are derived from an embryonic tetracarcinoma in mice and readily differentiate into neuronal cells[34] in the presence of retinoic acid (RA). As part of the study, the effect of the excitation signal frequency and the interrogation parameters for different testing scenarios were also investigated. Our findings clearly establish the feasibility of the microfluidic impedance FC for non-invasive, label-free characterization of the differentiation state of the stem cells.

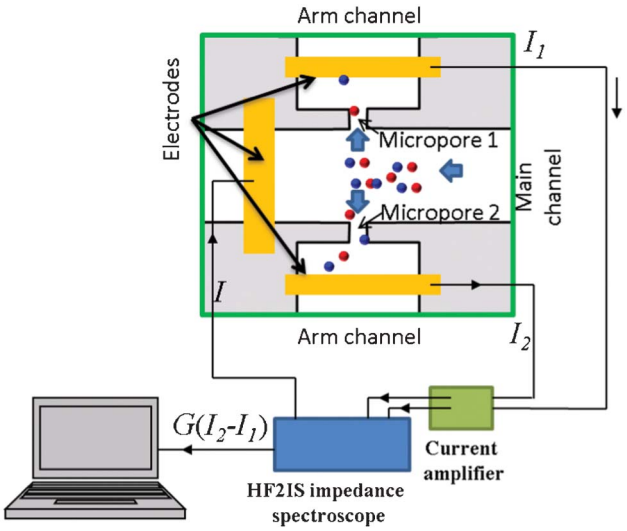

Fig. 1 Schematic of principle and microfluidic impedance FC design. The device consists of a main channel connected with two arm channels through micropores. AC signal is applied between the electrode in the main channel and the two side electrodes (located within the arm channels). A current amplifier is used to convert the current signal into the voltage signal. The acquired data is sent to a computer for the post process.

This paper is organized as follows: the principle and design of the microfluidic impedance FC device are first described in Section 2; materials and methods, such as sample preparation, device fabrication, measurement protocol, and experimental setup are elucidated in Section 3; results and discussion of the experimental testing and device and algorithm performance are presented in Section 4; and the paper is concluded with a summary of our technical findings and conclusions in Section 5.

2 Principle and design

In this section, we present the principle and design of our microfluidic impedance FC based on the dual micropore configurations. The device consists of a main horizontal channel and two arm channels, which, respectively, lead to a sample inlet and two arm outlets (see Fig. 1). The main horizontal channel and the arm channels are connected by two micropores. Two micro-electrodes are located within the arm channels and a third micro-electrode is located downstream of the main channel; these three electrodes together are utilized for impedance measurements as described below.

During experimental testing, both electrodes located within the arm channels are excited with the same AC signal (both amplitude and phase). The current I, originating from the electrode in the main channel, is split into two parts I_1 and I_2, which correspond to the current passing through micropore 1

and micropore 2, respectively. The difference between these two currents ($I_2 - I_1$) is amplified and converted into a voltage signal $G(I_2 - I_1)$ using a current amplifier with a gain factor G. The converted signal is then sent to the computer for recording and analysis. If there is no cell passing through the micropores, the differential current ($I_2 - I_1$) remains constant. Such a dual micropore design not only doubles the throughput but also allows each individual pore to be used as the reference for the other pore. Note that each micropore makes the major contribution to the overall impedance of the corresponding arm channel due to its distinctly small size. Meanwhile, the cell carries markedly different impedance from the medium solution in the channel due to its electrophysiological behavior. Both these factors combine to give rise to a significant variation in the impedance and the associated current as a cell traverses the micropore, which consequently generates a positive or a negative spike in the measured differential voltage $G(I_2 - I_1)$. The sign of the spike depends on the configurations of the electrode connection. It should be pointed out that the probability for two cells to pass through both micropores simultaneously is low in practice (about 0.01% in our measurement) and can be neglected by using sufficiently dilute cell concentrations. The measured voltage signal indicative of the impedance variations contains rich information of the biophysical properties of the particles, including size, double layer capacitance, membrane capacitance, cytoplasm resistance *etc*. Therefore, it can be used to interrogate the unique features of the cells (*e.g.*, differentiation state) that normally produce significant changes in morphology and membrane structure of the cells.

3 Materials and methods

3.1 Sample preparation

Mouse embryonic carcinoma cell lines P19 (ATCC# CRL-1825) were cultured in gelatin-coated flasks in alpha-Minimum Essential Media (αMEM, Mediatech, Inc.) supplemented with 2.5% fetal bovine serum, 7.5% bovine calf serum, 500 U mL^{-1} of penicillin–streptomycin and maintained at 5% CO_2 and 37 °C. Confluent cells were trypsinized and sub-cultured in well plates for immunohistochemical staining and monitoring. The cells were treated with a differentiation induction media αMEM supplemented with 1 μM retinoic acid (RA), 2.5% FBS, and 500 U mL^{-1} of penicillin–streptomycin to induce differentiation towards a neuronal lineage. Cells were maintained at 5% CO_2 and 37 °C, and the differentiation state was optically monitored daily using both phase contrast and fluorescence microscopy.

Immunohistochemical staining for microtubule-associated protein 2 (MAP2), expressed in differentiated cells and octamer-binding transcription factor 4 (OCT-4), expressed in undifferentiated cells was performed using previously published methods.[35] Briefly, P19 cells were fixed in 4% formaldehyde on ice, permeabilized in 0.1% Triton X-100, quenched with 2% BSA in PBS, and then incubated overnight with MAP2 (1 : 500 dilution, Sigma Aldrich) and OCT-4 (1 : 200 dilution, Santa Cruz Biotechnology, Inc) at 4 °C. The cells were subsequently washed with PBS followed by incubation with a secondary antibody (FITC conjugated anti-mouse IgG, 1 : 150 dilution, or TRITC conjugated IgG, 1 : 100 dilution, Sigma Aldrich) for 2 h at room temperature. Fig. 2 shows the phase contrast, MAP2 stained, OCT-4 stained images of both undifferentiated and differentiated P19 tetracarcinoma cells after 11 days culture. On day 11, P19 cells were trypsinized and resuspended in αMEM media. In addition to P19 tetracarcinoma cells, a non-biological poly-

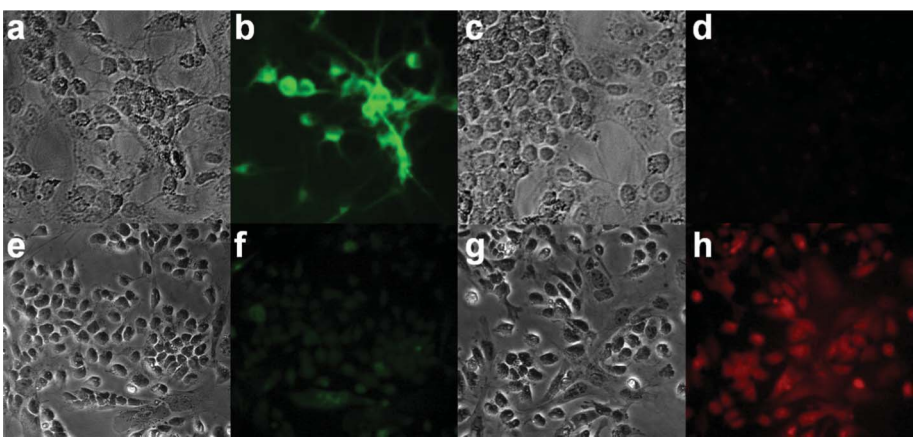

Fig. 2 Microscope images of differentiated and undifferentiated P19 cells. (a) Phase contrast image of differentiated cells; (b) microtubule-associated protein 2 (MAP2) stained image of differentiated cells shown in ''a''; (c) phase contrast image of differentiated cells; (d) octamer-binding transcription factor 4 (OCT-4) stained image of differentiated cells shown in ''c''; (e) phase contrast image of undifferentiated cells; (f) MAP2 stained image of undifferentiated cell shown in ''e''; (g) phase contrast image of undifferentiated cells; (h) OCT-4 stained image of undifferentiated cells shown in ''g''. MAP2 expressed in differentiated P19 cells showed strong intensity after 11 days culture compared to minimal intensity in undifferentiated cells, while OCT-4 expressed in undifferentiated cells showed high intensity compared to undetectable levels in differentiated cells. Note the clearly visible dendrites in the differentiated cells (phase contrast and MAP2 stained).

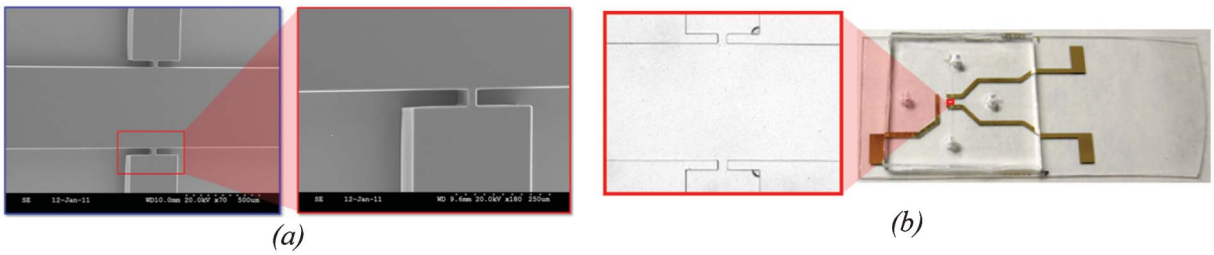

Fig. 3 Fabrication of the microfluidic impedance FC device: (a) SEM image of the SU8 master with micropores. PDMS microchannels are cast from the SU-8 master using soft lithography; (b) Assembled device including PDMS channels bonded on lithographically patterned gold-on-glass electrodes and contact pads.

styrene beads suspension (Duke Standards* 4000 Series Monosized Particles with diameter 20 μm, Thermo Scientific) was used in experimental testing for characterizing the system. The bead is similar in size to P19 cells that has an average size of approximately 17 μm in suspension.

3.2 Device fabrication

The microfluidic device consisted of two complementary layers: (1) a fluidic channel layer for flowing in the cell sample and (2) a gold electrode layer on a glass substrate for performing impedance measurements. The microfluidic channels were fabricated in PDMS using soft lithography techniques and the gold electrodes were fabricated using standard lithography techniques.[36] To assemble the device, the PDMS layer was bonded onto the glass/electrode slide using plasma bonding. Fig. 3a shows the SU8 master consisting of a main horizontal microchannel and two vertical arm channels, and Fig. 3b shows the assembled microfluidic chip. The widths of the main channel and arm channels are 500 μm and 320 μm, respectively, and the channel depth is 27 μm. The geometric size of the micropore is 40 μm × 40 μm.

3.3 Measurement protocol and experimental setup

The experimental setup is illustrated in Fig. 4. A syringe pump (PHD 22/2000, Harvard Apparatus) was used to pump the stem cell solution into the microfluidic device. During experiments the reservoir located downstream of the main channel was closed by a mechanical valve to divert the cells towards the micropores. An HF2IS impedance spectroscope (Zurich Instruments AG) was used to measure the impedance signal. During the measurement, the arm outlets were open. The injected cells passed through the micropores and the impedance signals were then collected according to the aforementioned protocol. A digital camera (CoolSNAP HQ2, Photometrics) was used for cell visualization, images recording, and cross-examination between the collected impedance data and optical data. The concentration of the P19 cells and the polystyrene beads were comparable and approximately $\sim 10^5$ particles per mL. The total volume of the mixed sample was 2 μL and the impedance measurements took 5 min per test.

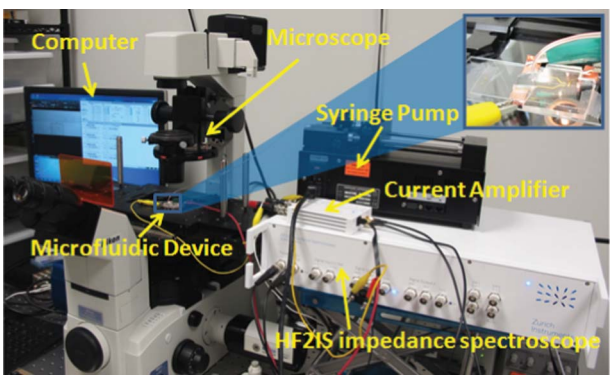

Fig. 4 Instrumentation of the experimental testing. The key instruments include the current amplifier and HF2IS impedance spectroscope (Zurich Instruments AG).

3.4 Signal processing and data analysis algorithm

The recorded impedance signals were first preprocessed with data detrending and filtration to improve signal quality. A peak detection approach was developed to detect the spike and calculate the spike amplitude and transit time. A signal processing algorithm based on a machine learning method-support vector machine (SVM) was used for categorization/classification of the measured signals to differentiate and identify the samples. SVM is a class of supervised machine learning methods used for data classification and regression problems.[37] SVM is a promising alternative to ANN for classifying impedance data from different cells and circumventing ANN's drawbacks, such as local minimal convergences and complex network configuration.

The principle of SVM is to train a model with the given inputs x_i (*e.g.*, the amplitude value of the voltage spike or other impedance relevant parameters) and the given output y_i (two classes such as 1 or −1) by solving the following optimization problem.

$$\begin{aligned} &\min_{\omega,b,\xi} \quad \frac{1}{2}\omega^T\omega + C\sum_{i=1}^{l}\xi_i \\ &\text{subject to } y_i(\omega^T\phi(x_i)+b) \geq 1-\xi_i, \quad \xi_i \geq 0, i=1,\ldots,l, \end{aligned} \tag{1}$$

where $\phi(x_i)$ maps x_i into a higher dimensional space and $C > 0$ is the regularization parameter. Due to the possible high dimensionality of ω, we solve the following dual problem instead of the original eqn (1):

$$\begin{aligned} &\min_{\alpha} \quad \frac{1}{2}\alpha^T Q\alpha - e^T\alpha \\ &\text{subject to } y^T\alpha = 0, \quad 0 \leq \alpha_i \leq C, \quad i=1,\ldots,l, \end{aligned} \tag{2}$$

where $e = [1,...,1]^T$ and Q is a positive semi-definite matrix, $Q = y_i y_j K(x_i,x_j)$ and $K = \phi(x_i)^T\phi(x_j)$ is the kernel function. Radial basis function (RBF) is selected as the kernel function in this study. After problem (2) is solved, the optimal ω satisfies

$$\omega = \sum_{i=1}^{l} y_i \alpha_i \phi(x_i) \tag{3}$$

and the design function

$$\mathrm{sgn}(\omega^T\phi(x)+b) = \mathrm{sgn}(\sum_{i=1}^{l} y_i \alpha_i K(x_i,x)+b) \tag{4}$$

is used to identify or classify the outputs.

Practically, the SVM-based signal processing algorithm was implemented and used as follows: (i) we first took two impedance measurements that, separately, used different samples (*e.g.*, cells *vs.* polystyrene beads) to generate the training and validation data, where both inputs (the measured signal) and outputs (that is, the category of the sample, *e.g.*, 1 for cell and −1 for beads) were known; (ii) the training and validation data was used to train the SVM classification engine and examine its accuracy, respectively; and (iii) a test using the mixed sample of both cells was performed, where only inputs were known and outputs were unknown. We predicted the output values using the trained SVM engine, *viz.*, classifying the measurements into the corresponding category. A SVM library, LIBSVM (http://www.csie.ntu.edu.tw/~cjlin/libsvm),[37] was used in the algorithm development. The algorithms for data analysis were all implemented on Matlab® (2011a, MathWorks).

4 Results and discussion

4.1 Measurements of impedance signals

To demonstrate the process of measuring the impedance signal, three experimental tests were undertaken at a frequency of 50 kHz. The first and the second tests used the sample solution containing only the polystyrene beads or the undifferentiated P19 cells, respectively, and a third test employed a mixed sample consisting of both beads and cells.

Fig. 5a illustrates the measurement results of 20 μm beads, in which a negative and a positive spike were observed when a bead passed through the bottom micropore and the top micropore (see the images on the left and right side), respectively. Similar results were observed for undifferentiated P19 cells (Fig. 5b) with the only difference being that the spike amplitude of the undifferentiated P19 cell was smaller. The results of the third experiment, using a mixed sample (Fig. 5c), clearly exhibit spikes with both the large and small amplitudes, corresponding to the 20 μm beads and P19 cells, respectively, which can be used to qualitatively distinguish both populations. The histogram of the amplitude *vs.* the number of occurrences for both particles is presented in Fig. 5d. We can see that the amplitude for 20 μm beads is noticeably larger than that for P19 cells, and the mean and standard deviation for them were 1.24 ± 0.1 mV and 0.54 ± 0.2 mV, respectively.

4.2 Identification of undifferentiated P19 cells and polystyrene beads

Given the two distinct populations in Fig. 5d, the signal processing and data analysis algorithm based on SVM was employed to demarcate a classification boundary for resolving them. To evaluate its performance, a microfluidic impedance FC test was conducted with simultaneous application of four different frequencies (50 kHz, 250 kHz, 500 kHz and 1 MHz) at the electrodes. In order to gain more insight into the experimental data, the detected impedance signal was split into real and imaginary parts, which collectively manifest the resistive and capacitive contributions of the particles to the overall impedance signal, and can be used to interrogate the frequency-dependent biophysical properties.

Fig. 6 illustrates the training data (the left column) and the identification results (the right column) at different frequencies. The training data was generated by combining the separate testing results of 20 μm beads (colored in blue) and undifferentiated P19 cells (in red). It clearly shows that the real part of the data remains almost the same in the given frequency range because it is largely dominated by resistance of the particles, which is frequency independent. In contrast, the imaginary part grows dramatically (from 10^{-5} to 10^{-3} V) as the frequency dependent capacitive component plays an important role. The identification results indicate that the SVM model works very well in terms of distinguishing undifferentiated P19 cells and beads (98 signals in total) at all frequencies as shown in Fig. 6. The numbers of the beads and P19 cells identified by our SVM algorithm match very well at all frequencies as shown in Table 1 (52–55 for beads and 43–46 for P19 cells, comparable to the theoretical calculation using approximate concentration and volume above), confirming salient consistency among all microfluidic impedance FC tests and the reliability of our signal processing and data analysis for particle detection.

4.3 Identification of undifferentiated and differentiated P19 cells

The identification of differentiated and undifferentiated P19 cells poses a significant challenge as their size and electrical behavior in the resistance-dominant regime are comparable, in contrast to the case above. This was confirmed by the impedance measurement of both undifferentiated and differentiated P19 cells at 50 kHz (see Fig. 7a). We can see that the real and imaginary parts of the signal from both populations scatter in a broad region and overlap to a great extent, which makes the distinction difficult as confirmed in their histogram curves of the amplitude *vs.* number in Fig. 7b. The value of the imaginary part is at least 1–2 order less than that of the real part, confirming the dominant resistive behavior in the impedance response at this frequency range.

Since the membrane capacitance can change during cell differentiation, a more appropriate means to identify the differentiation state is to measure their impedance response in the capacitance-dominant regime,[19] which can be accomplished by using a higher frequency in the AC excitation

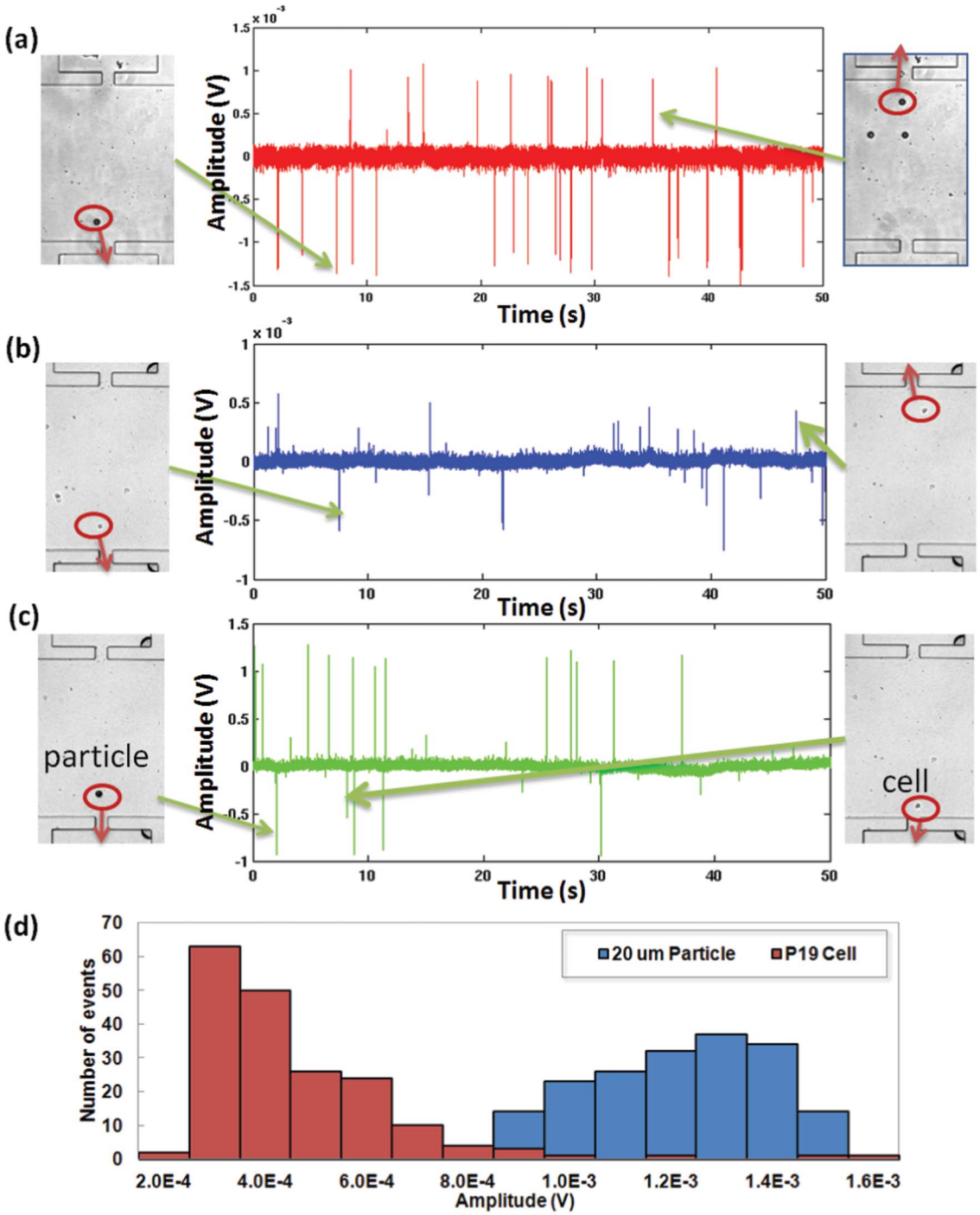

Fig. 5 Experimental testing of 20 μm beads and undifferentiated P19 cells: sample containing (a) only 20 μm polystyrene beads; (b) only undifferentiated P19 cells, and (c) mixed sample of both beads and P19 cells; (d) histogram of the spike amplitude *vs.* number of occurrences for the undifferentiated P19 cells and 20 μm polystyrene beads.

signals. As the frequency increases, the frequency-dependent capacitive behavior of the membrane structures makes a significant contribution to the measured impedance signal. Two separate tests, using either differentiated or undifferentiated P19 cells, were performed using AC excitation with four different frequencies (50 kHz, 250 kHz, 500 kHz and 1 MHz) applied simultaneously at the electrodes. For signal processing, we introduced another interrogation parameter – opacity,[38] which is defined as the ratio of the measured signal amplitude at high frequency to that at low frequency – to normalize the raw data. A salient feature of opacity is that it is almost independent of cell size and mitigates data scatter

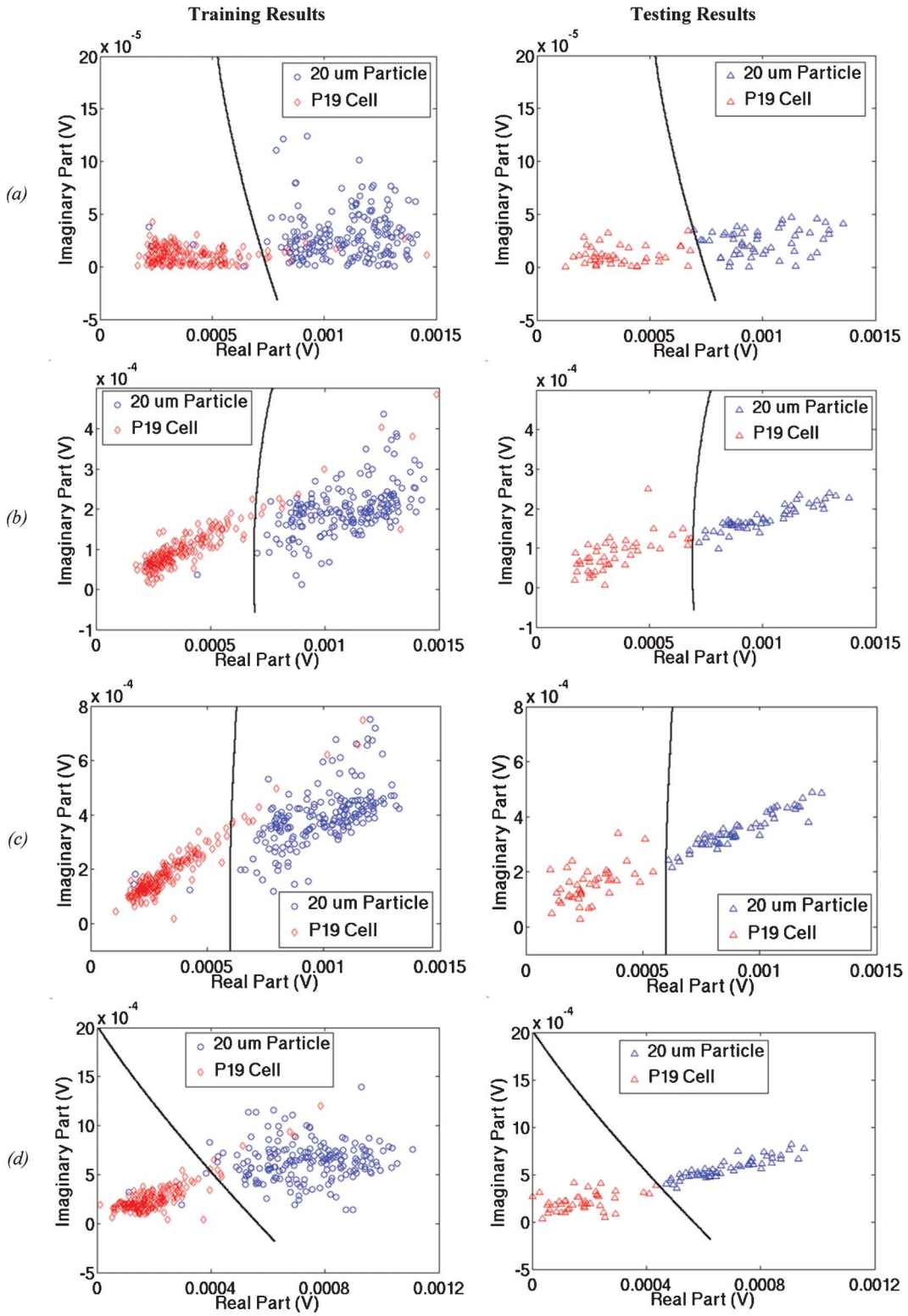

Fig. 6 Differentiation of bead and undifferentiated P19 cell using the SVM classification engine. Real and imaginary parts of the impedance signal were used as the interrogation parameters. Training data (left column) and identification results (right column) at (a) 50 kHz; (b) 250 kHz; (c) 500 kHz; (d) 1 MHz. The solid black curve represents the classification boundary determined by the SVM algorithm.

caused by the position of the cells relative to the electrodes, and hence, it effectively represents the interior dielectric properties of cells.

Fig. 8a–c illustrates the opacity of both differentiated and undifferentiated P19 cells at 250 kHz, 500 kHz and 1 MHz *vs.* the signal amplitude measured at low frequency (50 kHz)

Table 1 Summary of the total number of identified beads and undifferentiated P19 cells

	Interrogation parameters			
	Real part *vs.* imaginary part (under different frequencies)			
	50 kHz	250 kHz	500 kHz	1 MHz
Beads	53	53	55	55
P19 cells	45	45	43	43

using the training data consisting of pure populations, either differentiated (colored in blue) or undifferentiated cells (in red). It clearly shows that the opacity was almost similar at 250 kHz for both populations. Although a slight difference in opacity between the two populations was observed when the frequency was doubled to 500 kHz, the overlap between them was still noticeable. Finally, most of the differentiated and undifferentiated P19 cells could be distinguished from one another successfully when the frequency was increased to 1 MHz. Similar to those in typical non-invasive impedance measurements,[39,40] the voltage and current in our experiment are, respectively, 100 mV and at the nA level. The opacity for the differentiated cells was primarily in the range [0.2, 0.6], while the opacity for the undifferentiated cells fell between [0.6, 1.2], which can be used as a thresholding criterion to classify both populations. A more accurate way to attain the classification boundary and distinguish the differentiated and undifferentiated P19 cells is to use the SVM-based signal processing algorithm. As shown in Fig. 8c the differentiated and undifferentiated cells are separated by the solid black curve, the classification boundary determined by the SVM algorithm, yielding an accuracy level of 87%.

Fig. 8d illustrates the testing results obtained using a mixed sample measured at 1 MHz based on the classification boundary in Fig. 8c. A total number of 176 impedance signals were collected and analyzed, in which 143 symbols (△) in red located above the boundary were counted as undifferentiated P19 cells and the other 33 symbols in blue beneath were differentiated cells. It should be pointed out that although all the results of the signal processing and data classification below are for two sample categories, the approach can be readily extended to multiple cell types.

5 Conclusions

We have developed a non-invasive, label-free, micropore-based microfluidic impedance FC for single cell property characterization, in particular, distinction between the non-biological *vs.* biological cells, and identification of the differentiation state of the stem cells. The novel dual micropore and associated electrode design assume dual roles: scaling up the processing throughput and providing a reference electrode for one another. A signal processing algorithm based on the support vector machine (SVM) theory and the data classification method was developed to enable the identification of the cell types and differentiation state based on the measured impedance values. The experimental testing was carried out at multiple excitation frequencies (50 kHz, 250 kHz, 500 kHz, and 1 MHz) to characterize the performance of the microfluidic impedance FC device and the SVM signal processing algorithm. Important technical findings include:

(1) To distinguish undifferentiated embryonic cells and non-biological 20 μm polystyrene beads, the real and the imaginary part of the amplitude of the voltage spike was used as the interrogation parameter to accentuate the size effects. Salient differences in impedance signatures of both samples were obtained at all the testing frequencies. The SVM signal processing algorithm was employed to derive the classification boundary, which achieves 95% accuracy among all the tests.

(2) Resolving the undifferentiated and differentiated embryonic cells was not feasible in low-to-medium excitation frequency. This was mainly attributed to the comparable sizes near the resistance-dominant regime. Therefore, high frequency (1 MHz) measurements were needed to focus the investigation on the capacitive components in the impedance response. The opacity served as the interrogation parameter to mitigate data scattering due to the heterogeneity of cell size in the population. The determined classification boundary determined by the SVM algorithm resulted in 87% accuracy.

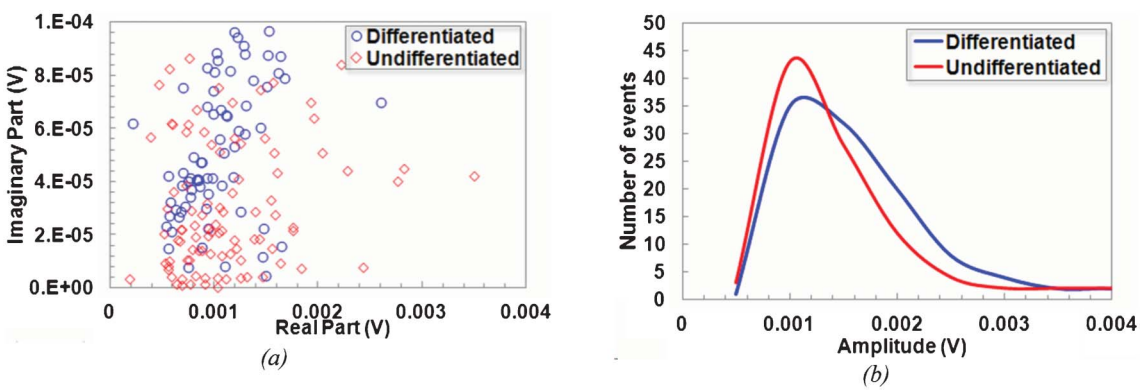

Fig. 7 (a) Real *vs.* imaginary part of the voltage spike during particle passage through the micropore at 50 kHz; (b) histogram of the amplitude *vs.* number of occurrences for the differentiated and undifferentiated P19 cells at 50 kHz.

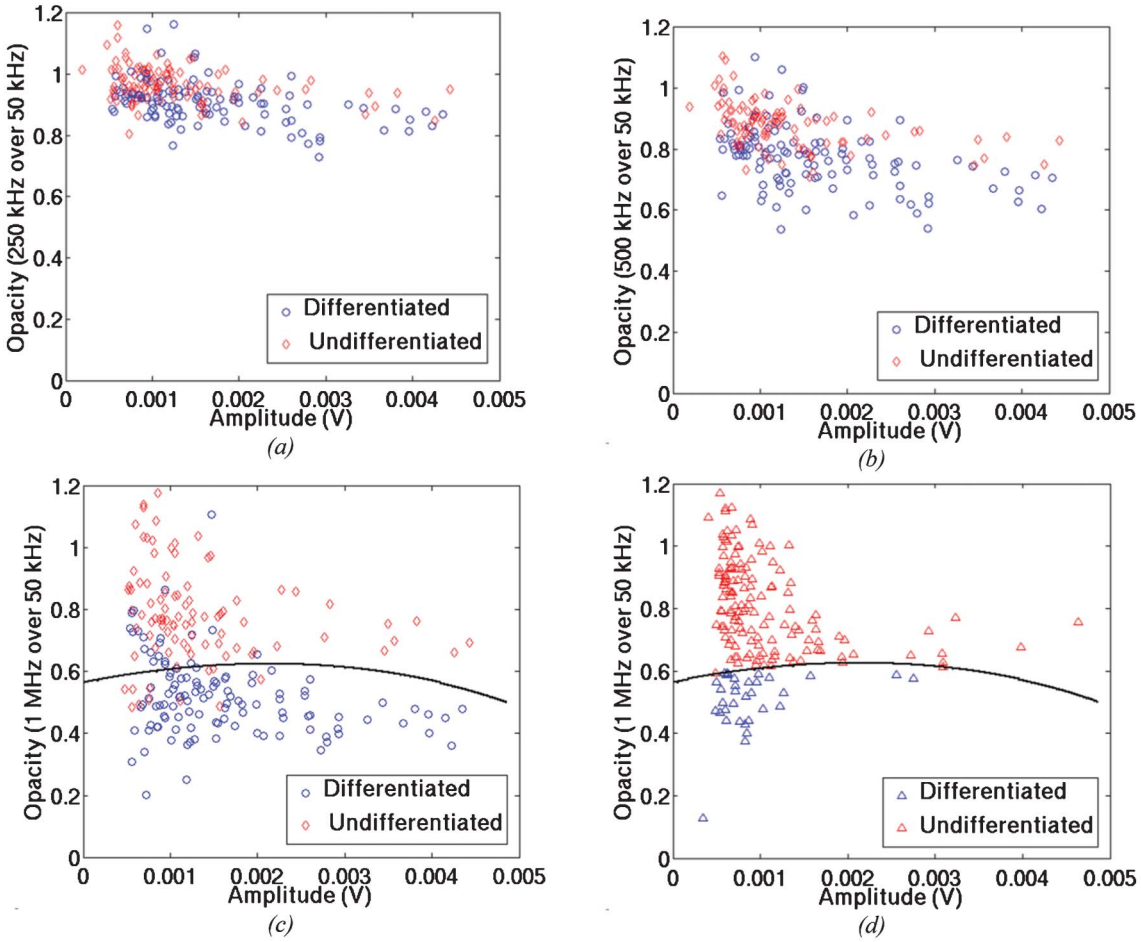

Fig. 8 Measured opacity *vs.* the amplitude at 50 kHz at different frequencies: (a) 250 kHz; (b) 500 kHz; (c) 1 MHz. These data are generated using the training data consisting of pure populations, either differentiated (colored in blue) or undifferentiated cells (in red). There is significant overlap in the opacity values at 250 kHz and even 500 kHz. However, the opacity values for differentiated and undifferentiated cells are significantly different at 1 MHz frequency. The solid black curve in (c) represents the classification boundary determined by the SVM algorithm. (d) Identification of differentiated and undifferentiated P19 cells using a mixed sample with both differentiated and undifferentiated stem cells using opacity at 1 MHz over 50 kHz and SVM-based classification.

Our studies firmly establish the feasibility of the microfluidic impedance FC for non-invasive, label-free identification of the differentiation state of the stem cells. In addition, the well-established technique can be readily extended to identify small size particles and cells by scaling the pore size appropriately, which may significantly benefit the detection of bacteria and pathogens for medical diagnostics and biodefense applications. Future developments will focus on improving the identification accuracy and the processing throughput,[41] and developing the impedance activated cell sorting functionalities.

Acknowledgements

This research was sponsored by the U.S. Army Medical Research and Materiel Command (USAMRMC) under SBIR contract No. W81XWH-12-C-0069.

References

1 H. Hentze, R. Graichen and A. Colman, Cell therapy and the safety of embryonic stem cell-derived grafts, *Trends Biotechnol.*, 2007, **25**(1), 24–32.
2 J. Y. Yu, *et al.*, Induced pluripotent stem cell lines derived from human somatic cells, *Science*, 2007, **318**(5858), 1917–1920.
3 J. Cai, *et al.*, Assessing self-renewal and differentiation in human embryonic stem cell lines, *Stem Cells*, 2006, **24**(3), 516–530.
4 A. Castagnola, S. Eda and J. L. Jurat-Fuentes, Monitoring stem cell proliferation and differentiation in primary midgut cell cultures from *Heliothis virescens* larvae using flow cytometry, *Differentiation*, 2011, **81**(3), 192–198.
5 I. Giaever and C. R. Keese, Monitoring fibroblast behavior in tissue culture with an applied electric field, *Proc. Natl. Acad. Sci. U. S. A.*, 1984, **81**(12), 3761.
6 I. Giaever and C. R. Keese, Use of electric fields to monitor the dynamical aspect of cell behavior in tissue culture, *IEEE Trans. Biomed. Eng.*, 1986, **2**, 242–247.

7 C. M. Lo, C. R. Keese and I. Giaever, Monitoring motion of confluent cells in tissue culture, *Exp. Cell Res.*, 1993, **204**(1), 102–109.
8 I. Giaever and C. R. Keese, Micromotion of mammalian cells measured electrically, *Proc. Natl. Acad. Sci. U. S. A.*, 1991, **88**(17), 7896.
9 I. Giaever and C. R. Keese, A morphological biosensor for mammalian cells, *Nature*, 1993, **366**(6455), 591.
10 J. H. T. Luong, *et al.*, Monitoring motility, spreading, and mortality of adherent insect cells using an impedance sensor, *Anal. Chem.*, 2001, **73**(8), 1844–1848.
11 C. Xiao, *et al.*, Assessment of cytotoxicity using electric cell-substrate impedance sensing: concentration and time response function approach, *Anal. Chem.*, 2002, **74**(22), 5748–5753.
12 H. E. Park, *et al.*, Real-Time Monitoring of Neural Differentiation of Human Mesenchymal Stem Cells by Electric Cell-Substrate Impedance Sensing, *J. Biomed. Biotechnol.*, 2011, **2011**(1), 485173.
13 E. Bieberich and A. Guiseppi-Elie, Neuronal differentiation and synapse formation of PC12 and embryonic stem cells on interdigitated microelectrode arrays: Contact structures for neuron-to-electrode signal transmission (NEST), *Biosens. Bioelectron.*, 2004, **19**(8), 923–931.
14 C. Hildebrandt, *et al.*, Detection of the osteogenic differentiation of mesenchymal stem cells in 2D and 3D cultures by electrochemical impedance spectroscopy, *J. Biotechnol.*, 2010, **148**(1), 83–90.
15 C. Dalmay, *et al.*, Ultra sensitive biosensor based on impedance spectroscopy at microwave frequencies for cell scale analysis, *Sens. Actuators, A*, 2010, **162**(2), 189–197.
16 P. O. Bagnaninchi and N. Drummond, Real-time label-free monitoring of adipose-derived stem cell differentiation with electric cell-substrate impedance sensing, *Proc. Natl. Acad. Sci. U. S. A.*, 2011, **108**(16), 6462.
17 Y. Cho, *et al.*, Whole-cell impedance analysis for highly and poorly metastatic cancer cells, *J. Microelectromech. Syst.*, 2009, **18**(4), 808–817.
18 T. Sun and H. Morgan, Single-cell microfluidic impedance cytometry: a review, *Microfluid. Nanofluid.*, 2010, **8**(4), 423–443.
19 S. Gawad, L. Schild and P. Renaud, Micromachined impedance spectroscopy flow cytometer for cell analysis and particle sizing, *Lab Chip*, 2001, **1**(1), 76–82.
20 S. Gawad, *et al.*, Dielectric spectroscopy in a micromachined flow cytometer: theoretical and practical considerations, *Lab Chip*, 2004, **4**(3), 241–251.
21 K. Cheung, S. Gawad and P. Renaud, Impedance spectroscopy flow cytometry: On-chip label-free cell differentiation, *Cytometry, Part A*, 2005, **65**(2), 124–132.
22 C. Küttel, *et al.*, Label-free detection of Babesia bovis infected red blood cells using impedance spectroscopy on a microfabricated flow cytometer, *Acta Trop.*, 2007, **102**(1), 63–68.
23 D. Holmes, *et al.*, Leukocyte analysis and differentiation using high speed microfluidic single cell impedance cytometry, *Lab Chip*, 2009, **9**(20), 2881–2889.
24 D. Holmes and H. Morgan, Single cell impedance cytometry for identification and counting of CD4 T-cells in human blood using impedance labels, *Anal. Chem.*, 2010, **82**(4), 1455–1461.
25 A. Pierzchalski, *et al.*, Label-free hybridoma cell culture quality control by a chip-based impedance flow cytometer, *Lab Chip*, 2012, **12**(21), 4533–4543.
26 H. L. Gou, *et al.*, Label-free electrical discrimination of cells at normal, apoptotic and necrotic status with a microfluidic device, *J. Chromatogr., A*, 2011, **1218**(33), 5725–5729.
27 C. Bernabini, D. Holmes and H. Morgan, Micro-impedance cytometry for detection and analysis of micron-sized particles and bacteria, *Lab Chip*, 2011, **11**(3), 407–412.
28 O. A. Saleh and L. L. Sohn, Quantitative sensing of nanoscale colloids using a microchip Coulter counter, *Rev. Sci. Instrum.*, 2001, **72**(12), 4449–4451.
29 D. Satake, *et al.*, A sensor for blood cell counter using MEMS technology, *Sens. Actuators, B*, 2002, **83**(1), 77–81.
30 Y. Zheng, *et al.*, High-throughput biophysical measurement of human red blood cells, *Lab Chip*, 2012, **12**(14), 2560–2567.
31 Y. Zheng, *et al.*, Microfluidic characterization of specific membrane capacitance and cytoplasm conductivity of single cells, *Biosens. Bioelectron.*, 2013, **42**, 7.
32 C. van Berkel, *et al.*, Integrated systems for rapid point of care (PoC) blood cell analysis, *Lab Chip*, 2011, **11**(7), 1249–1255.
33 J. Chen, *et al.*, Classification of cell types using a microfluidic device for mechanical and electrical measurement on single cells, *Lab Chip*, 2011, **11**(18), 3174–3181.
34 M. Endo, M. A. Antonyak and R. A. Cerione, Cdc42-mTOR signaling pathway controls Hes5 and Pax6 expression in retinoic acid-dependent neural differentiation, *J. Biol. Chem.*, 2009, **284**(8), 5107–5118.
35 V. Babuška, *et al.*, Characterization of P19 cells during retinoic acid induced differentiation, *Prague Medical Report*, 2010, **111**(4), 289–299.
36 H. Song, *et al.*, Chaotic mixing in microchannels via low frequency switching transverse electroosmotic flow generated on integrated microelectrodes, *Lab Chip*, 2010, **10**(6), 734–740.
37 C. C. Chang and C. J. Lin, LIBSVM: a library for support vector machines, *ACM Transactions on Intelligent Systems and Technology (TIST)*, 2011, **2**(3), 27.
38 R. A. Hoffman and W. B. Britt, Flow-system measurement of cell impedance properties, *J. Histochem. Cytochem.*, 1979, **27**(1), 234.
39 J. Chen, *et al.*, A microfluidic device for simultaneous electrical and mechanical measurements on single cells, *Biomicrofluidics*, 2011, **5**(1), 014113.
40 Y. Huang, *et al.*, Instantaneous, quantitative single-cell viability assessment by electrical evaluation of cell membrane integrity with microfabricated devices, *Sens. Actuators, A*, 2003, **105**(1), 31–39.
41 A. V. Jagtiani, J. Carletta and J. Zhe, A microfluidic multichannel resistive pulse sensor using frequency division multiplexing for high throughput counting of micro particles, *J. Micromech. Microeng.*, 2011, **21**(6), 065004.

